ACS OMEGA

http://pubs.acs.org/journal/acsodf

Article

Efficient Photo-Assisted Thermal Selective Oxidation of Toluene Using N-Doped TiO_2

Cheng Chen, Mingge Wu, Chunyan Ma, Maoyong Song,* and Guibin Jiang

Cite This: *ACS Omega* 2023, 8, 21026−21031

Read Online

ACCESS | Metrics & More | Article Recommendations | Supporting Information

ABSTRACT: Selective oxidation of toluene is a key reaction to produce high value-added products but remains a big challenge. In this study, we introduce a nitrogen-doped TiO_2 (N-TiO_2) catalyst to create more Ti^{3+} and oxygen vacancy (O_V), which act as active sites for selective oxidation of toluene via activating O_2 to superoxide radical ($\bullet O_2^-$). Interestingly, the resulting N-TiO_2-2 exhibited an outstanding photo-assisted thermal performance with a product yield of 209.6 mmol·g_{cat}^{-1} and a toluene conversion of 10960.0 μmol·g_{cat}^{-1}·h^{-1}, which are 1.6 and 1.8 times greater than those obtained under thermal catalysis. We showed that the enhanced performance under photo-assisted thermal catalysis was attributed to more active species generation by making full use of photogenerated carriers. Our work suggests a viewpoint to apply a noble-metal-free TiO_2 system in the selective oxidation of toluene under solvent-free conditions.

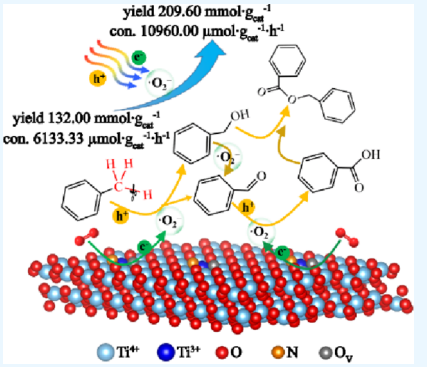

1. INTRODUCTION

Selective oxidation of toluene is a key transformation to form high-value products, including benzyl alcohol, benzaldehyde, benzoic acid, and benzyl benzoate. They are significant intermediates in the manufacture of pharmaceuticals, dyes, solvents, perfumes, plasticizers, preservatives, and flame retardants.[1−3] Disappointingly, it is usually necessary to add solvents in the process of preparing high value-added products, and the generated products often have the problem of chlorine residue.[4−8] These not only cause serious environmental problems but also limit the scope of use of the products.[9,10] Thus, it is a promising choice for direct selective oxidation of toluene with O_2 as oxidant without solvent. Indeed, under solvent-free conditions, both thermocatalysis and photocatalysis can achieve selective oxidation of toluene to obtain high value-added products.[11−16] However, it also remains a range of significant challenges. The most urgent issues include the extremely low product yields and toluene conversion. For example, using the high-performance AuPd alloy catalyst, a low product yield of 59.5 mmol·g_{cat}^{-1} was obtained along with a poor toluene conversion of 2375.0 μmol·g_{cat}^{-1}·h^{-1}.[1] There is a need to design a catalyst with excellent performance for selective oxidation of toluene.

TiO_2, as a classic catalyst, has attracted much attention owing to its excellent photocatalytic performance, but it also shows excellent performance in the thermal catalytic reaction.[17−23] It can construct a great number of Ti^{3+} and oxygen vacancy (O_V) through further treatments, such as thermal reduction, semiconductor recombination, dye photosensitization, and doping.[24−26] The resulting O_V often acts as active site to activate O_2 to generate superoxide radical ($\bullet O_2^-$), and the obtained Ti^{3+} provides electrons in this process.[27] Considering that $\bullet O_2^-$ is the active species of the selective oxidation of toluene, TiO_2 with O_V and Ti^{3+} can catalyze the selective oxidation of toluene to obtain high-value products.[28,29] Combined with excellent optical property, TiO_2 may further enhance the catalytic performance via photo-assisted thermal catalysis.[30]

In this study, we aimed to create more O_V and Ti^{3+} on TiO_2 via optimizing nitrogen doping. The resulting nitrogen-doped TiO_2 (N-TiO_2) catalysts were used for selective oxidation of toluene without solvent under thermal, photo, and photo-assisted thermal catalysis. We demonstrated that the combination of light and heat can greatly enhance the catalytic performances of N-TiO_2 catalysts on selective oxidation of toluene owing to the increased O_V and Ti^{3+}, as well as their optimized optical properties.

2. EXPERIMENTAL SECTION

2.1. Chemicals. TiO_2 (Anatase) was purchased from Sigma Aldrich. Toluene and urea (99%) were purchased from Sinopharm Chemical Reagent Co., Ltd. Benzyl alcohol (99.5%), benzaldehyde (99.5%), benzoic acid (99.9%), benzyl benzoate (99.0%), o-xylene (96.0%), and absolute ethanol were purchased from Aladdin Biochemical Technology Co.,

Received: March 20, 2023
Accepted: May 19, 2023
Published: May 30, 2023

Ltd., Shanghai, China. All chemicals were used as received without any further purification.

2.2. Catalyst Preparation. N-TiO_2 was prepared by the impregnation method, and urea was used as the nitrogen source. In detail, 0.5 g of urea was dissolved in ultrapure water and then 1 g of TiO_2 was added and stirred for 5 h to obtain white suspension. Subsequently, the suspension was dried at 100 °C for 12 h and then calcined at 400 °C for 2 h with a heating rate of 3 °C/min after being ground. Finally, N-TiO_2-0.5 was achieved. N-TiO_2-X (X represents the mass ratio of urea to TiO_2, X = 0.5, 1, 1.5, 2, and 2.5, respectively) were synthesized using different amounts of urea.

2.3. Characterization. Characterizations are detailedly described in the Supporting Information.

2.4. Catalytic Reaction. *2.4.1. Thermal Selective Oxidation of Toluene.* Thermal selective oxidation of toluene was carried out in an autoclave (100 mL). Toluene (40 mL) and N-TiO_2 or pristine TiO_2 (100 mg) were added into the reactor and then purged with O_2 repeatedly. Subsequently, it was heated up to 160 °C, and O_2 was added to the reactor, reaching 1 MPa. Finally, the magnetic stirrer was turned on and the reaction was started. Test samples were taken before heating and after the reaction and analyzed by gas chromatography (2010Plus, Shimadzu, Japan).

2.4.2. Photo Selective Oxidation of Toluene. Toluene (40 mL) and N-TiO_2 or pristine TiO_2 (100 mg) were added into the reactor and purged with O_2 repeatedly. Then, it was irradiated with a 300 W Xe lamp, and O_2 was added to the reactor, reaching 1 MPa. Finally, the magnetic stirrer was turned on and the reaction was started. Test samples were taken before heating and after the reaction and analyzed by gas chromatography.

2.4.3. Photo-Assisted Thermal Selective Oxidation of Toluene. Toluene (40 mL) and N-TiO_2 or pristine TiO_2 (100 mg) were added into the reactor and purged with O_2 repeatedly. Then, it was heated up to 160 °C and irradiated with a 300 W Xe lamp. Finally, O_2 was added to the reactor to reach 1 MPa, the magnetic stirrer was turned on, and the reaction was started. Samples were taken before heating and after the reaction and analyzed by gas chromatography.

2.4.4. Quenching Experiment. In the thermal quenching experiment, compared to the thermal selective oxidation of toluene, only the initial feeding step is different, that is, toluene, catalyst, and quenching agent are added together, and the subsequent steps are completely the same. Similarly, in the photo-assisted thermal quenching experiment, compared to the photo-assisted thermal selective oxidation of toluene, only the initial feeding step is different, that is, toluene, catalyst, and quenching agent are added together, and the subsequent steps are completely the same.

3. RESULTS AND DISCUSSION

3.1. Morphology and Structure. N-TiO_2 was prepared by a facile impregnation method. X-ray diffraction (XRD) showed no changes in the peaks of the anatase phases (JCPDS No. #71-1166) (Figure 1a). Raman spectra showed that the signals were assigned to the E_g, E_g, B_{1g}, A_{1g}, and E_g modes of the anatase phase (Figure 1b).[31] Scanning electron microscopy (SEM) showed that N-TiO_2 and pristine TiO_2 had similar morphologies (Figure 1c and Figure S1), and SEM/energy-dispersive X-ray spectroscopy (EDS) confirmed that N was successfully doped into TiO_2 (Figure 1e and Figure S2). Transmission electron microscopy (TEM) and high-resolution

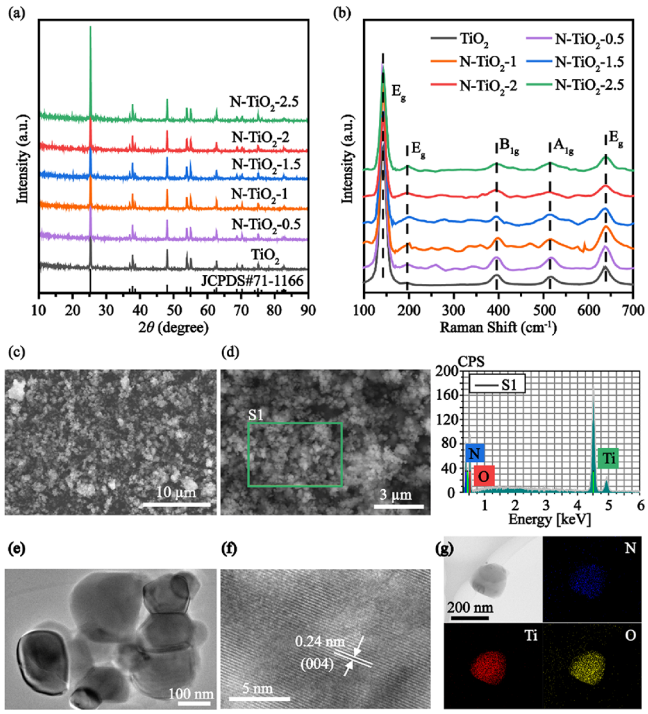

Figure 1. (a) XRD patterns and (b) Raman spectra of N-TiO_2 and pristine TiO_2. (c, d) SEM images and EDS spectra of N-TiO_2-2. (e) STEM, (f) HRTEM, and (g) elemental mappings of N, Ti, and O images of N-TiO_2-2.

transmission electron microscopy (HRTEM) revealed the crystal structures of N-TiO_2 and pristine TiO_2, and the lattice fringes with interplanar spacings of 0.24, 0.35, and 0.42 nm were assigned to (004), (101), and (120) from the TiO_2, respectively (Figure 1e,f and Figure S3).[32−34] SEM and TEM mapping images confirmed the homogeneous distribution of all elements in the N-TiO_2 and pristine TiO_2 (Figure 1g and Figures S4 and S5). All these indicate that N doping does not substantially change the original crystal phase structure of TiO_2.

The structure of N-TiO_2 was further characterized by X-ray photoelectron spectroscopy (XPS). The N 1 s spectra of N-TiO_2 had two characteristic peaks at 398.9 and 400.3 eV (Figure 2a), which corresponded to N−Ti−O and Ti−O−N bonds, respectively.[35−37] This is consistent with the result of Fourier transform infrared (FT-IR), where peaks at 978 and 1428 cm^{-1} corresponded to N−Ti−O and Ti−O−N bonds (Figure S6).[28] N−Ti−O indicates that N replaces the lattice O and bonds to Ti of TiO_2, while Ti−O−N represents the N doped into the interstitial site. As expected, the N atomic concentration increased in a sequence of N-TiO_2-0.5 < N-TiO_2-1 < N-TiO_2-1.5 < N-TiO_2-2 < N-TiO_2-2.5 according to the XPS results (Table S1). The Ti 2p spectra of N-TiO_2 and pristine TiO_2 had two peaks at 458.7 and 464.5 eV, which were attributed to Ti $2p_{3/2}$ and Ti $2p_{1/2}$, respectively (Figure 2b).[38,39] After Gaussian fitting, the peaks at 463.6 and 458.4 eV belonged to Ti^{3+}, and the peaks at 464.6 and 458.8 eV belonged to Ti^{4+}. Semiquantitative results showed that the Ti^{3+} content of N-TiO_2-2 (36.6%) was the largest among the N-TiO_2 and pristine TiO_2 (Table S2). The O 1s spectra of N-TiO_2 and pristine TiO_2 had three peaks at 532.5, 531.0, and 529.8 eV (Figure 2c), which belonged to OH groups, surface O_v, and lattice oxygen, respectively.[40] The O_v content of N-

https://doi.org/10.1021/acsomega.3c01887
ACS Omega 2023, 8, 21026−21031

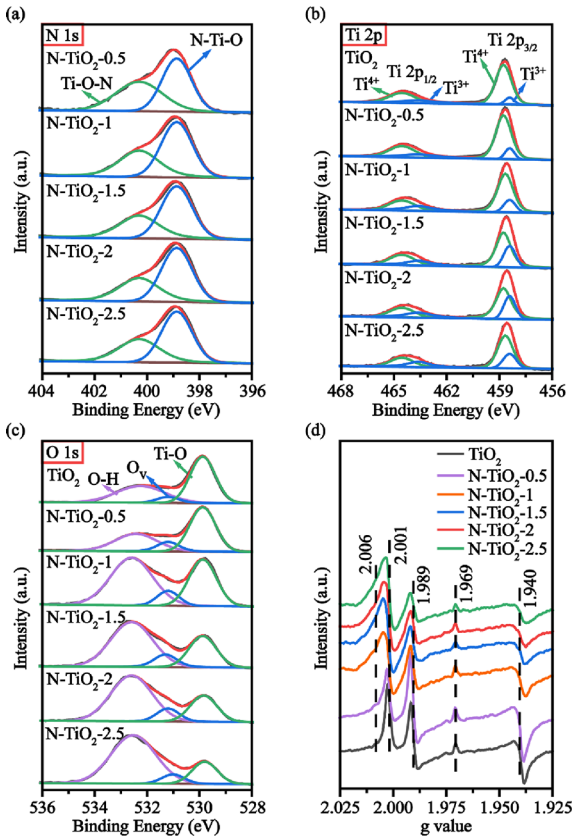

Figure 2. XPS spectra of (a) N 1s, (b) Ti2p, and (c) O 1s of N-TiO_2 and pristine TiO_2. (d) EPR spectra of N-TiO_2 and pristine TiO_2.

TiO_2-2 was the largest among the N-TiO_2 and pristine TiO_2, and the obtained $O_v/O_{O\text{-}Ti}$ value was 41.7% (Table S2).

The detect species containing unpaired electrons in N-TiO_2 were further characterized by electron paramagnetic resonance (EPR). There were four characteristic signals at g = 1.940, 1.969, 1.989, and 2.001, which were all belonged to Ti^{3+}. The signal at g = 2.001 belonged to the surface five coordination Ti^{3+} related to oxygen vacancy; the signal at g = 1.989 belonged to the bulk six coordination Ti^{3+}; the signal g = 1.969 belonged to the surface five coordination Ti^{3+} induced by H; and the signal g = 1.940 belonged to surface four coordination Ti^{3+}.[28] Another signal at g = 2.006 was attributed to O_v (Figure 2d).[41−43] Therefore, the N-TiO_2 and pristine TiO_2 both contained Ti^{3+} and O_v. However, the Ti^{3+} signals at g = 2.001 and 1.989 of N-TiO_2-1, N-TiO_2-1.5, N-TiO_2-2, and N-TiO_2-2.5 were broader than those of pristine TiO_2, which was due to more N doping and generation of more N-doped Ti^{3+}. The signal at g = 2.001 became broader because it was also overlapped with the gradually enhanced O_v signal at g = 2.006.

3.2. Photochemical Properties. The UV−vis diffuse reflectance spectra showed that N-TiO_2 absorbed light over a wide range from the ultraviolet to the visible light regions, and the spectrum of N-TiO_2-2 showed the most obvious red shift (Figure 3a), indicating the best light absorption and utilization. The optical band gaps of N-TiO_2, calculated based on the Tauc plot method, were narrower compared with that of pristine TiO_2, and N-TiO_2-2 had the narrowest band gap (Figure S7a), meaning the lowest excitation energy required from light. Combined with the valence bands deduced from the XPS spectra (Figure S7b), the positions of the conduction bands were determined, and the resulting electronic band

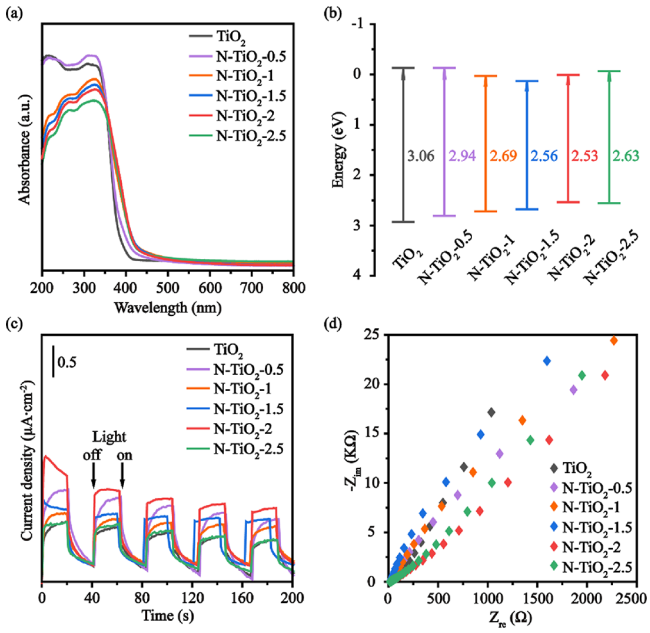

Figure 3. (a) UV−vis DRS spectra, (b) band structures, (c) photocurrent response, and (d) Nyquist plots of N-TiO_2 and pristine TiO_2.

structures of N-TiO_2 and pristine TiO_2 were plotted (Figure 3b). Furthermore, we detected the photocurrent response intensities of the N-TiO_2 and pristine TiO_2 and found that N-TiO_2-2 exhibited the best photocurrent response, thereby indicating good separation of the photogenerated electrons and holes (Figure 3c). Electrochemical impedance spectroscopy (EIS), which reflects the charge transfer resistance, was also performed, and N-TiO_2-2 was found to exhibit the smallest high-frequency semicircle in the Nyquist plot (Figure 3d), indicating the easiest carrier separation and transfer. Subsequently, the time-resolved fluorescence decay spectra of N-TiO_2 and pristine TiO_2 were used along with the corresponding lifetimes (τ) of the charge carriers to compare the charge separation efficiencies (Figure S8). As a result, it was found that N-TiO_2-2 exhibited the longest average lifetime (τ_a) of 7.53 ns, which corresponds to a higher charge separation efficiency. Overall, these results indicated that N-TiO_2 exhibited better optical property than pristine TiO_2, and the N-TiO_2-2 had the best separation and transport of the photogenerated electron−hole pairs.

3.3. Catalytic Performance. The thermo-, photo-, and photo-assisted thermocatalytic performances of N-TiO_2 and pristine TiO_2 for selective oxidation of toluene were investigated (Table S3). Under thermal catalysis, N-TiO_2 showed better catalytic performance than pristine TiO_2, and N-TiO_2-2 exhibited the optimal performance among the N-TiO_2 (Figure 4a). N-TiO_2-2 gave a product yield of 132.0 $mmol \cdot g_{cat}^{-1}$ and a toluene conversion of 6133.3 $\mu mol \cdot g_{cat}^{-1} \cdot h^{-1}$, which was 1.8 and 1.6 times those obtained over pristine TiO_2. Under photo catalysis, the yields of products were all less than 10.0 $mmol \cdot g_{cat}^{-1}$ and toluene conversions were also less than 700.0 $\mu mol \cdot g_{cat}^{-1} \cdot h^{-1}$ over N-TiO_2 and pristine TiO_2, with almost no activity (Figure 4a). Thus, the selective oxidation of toluene over N-TiO_2 and pristine TiO_2 is essentially thermally driven. Under photo-assisted thermal catalysis, the product yields and toluene conversions of N-TiO_2 and pristine TiO_2 had been significantly improved (Figure 4a),

https://doi.org/10.1021/acsomega.3c01887
ACS Omega 2023, 8, 21026−21031

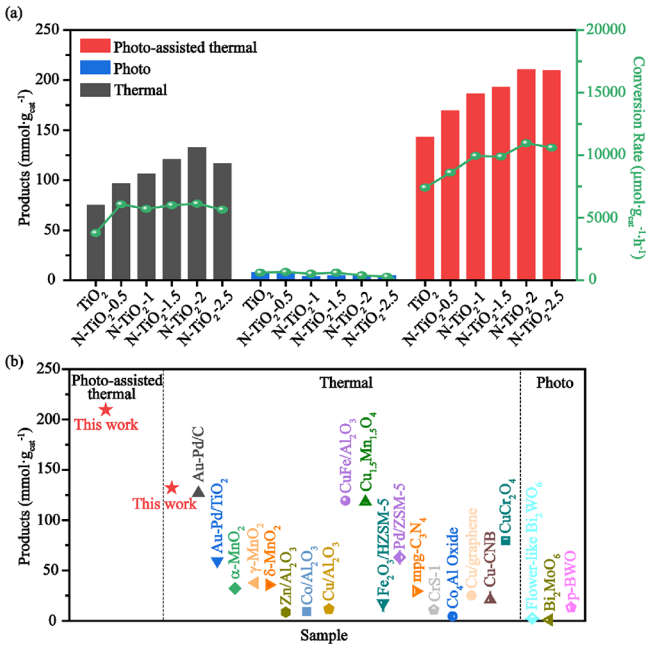

Figure 4. (a) Yields of the products and toluene conversions with N-TiO_2 and pristine TiO_2 under thermal (black), photo (blue), and photo-assisted thermal (red) catalysis conditions. (b) Comparison of the selective oxidation of toluene with the catalysts reported (Table S4).

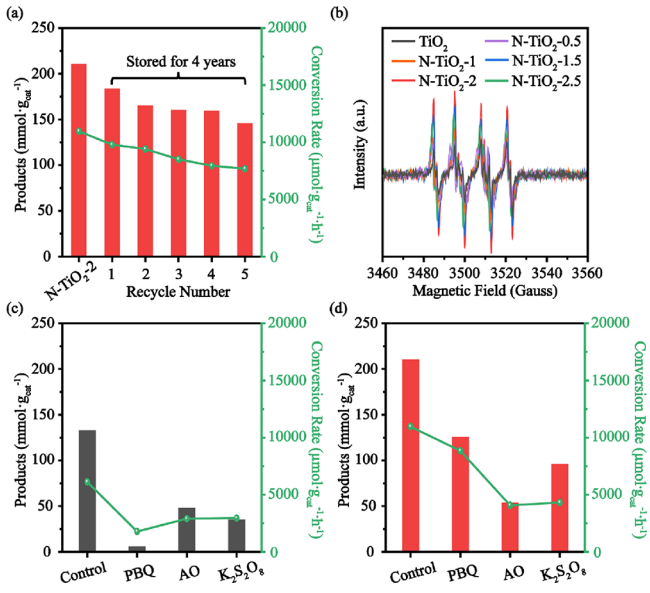

Figure 5. (a) Stability of N-TiO_2-2. (b) EPR spectra of $\bullet O_2^-$ from N-TiO_2 and pristine TiO_2 under light excitation. Product yields and toluene conversions over N-TiO_2-2 with the addition of quencher under (c) thermal catalysis or (d) photo-assisted thermal catalysis.

showing an excellent synergy between photo- and thermocatalysis. Similarly, the performance of N-TiO_2 was still superior to pristine TiO_2, and N-TiO_2-2 also exhibited the best performance among the N-TiO_2 (Figure 4a). N-TiO_2-2 showed the optimal performance with a product yield of 209.6 mmol·g_{cat}^{-1} and a toluene conversion of 10960.0 μmol·g_{cat}^{-1}·h^{-1}, which represents increases of 1.6 and 1.8 times, respectively, compared to its thermal catalytic performance. Further, the product yield and toluene conversion obtained over N-TiO_2-2 under the photo-assisted thermal catalysis were 1.5 and 1.5 times than those obtained over pristine TiO_2. The product yield of N-TiO_2-2 was also higher than most of the reported catalysts, and even higher than those over optimized Au−Pd catalysts (Figure 4b). Subsequently, using N-TiO_2-2 as a model catalyst, we further explored the effect of temperature on the activity and selectivity (Figure S9). The results showed that increasing the temperature helps to obtain more value-added products, but the effect on selectivity is not significant, mainly attributed to this being a thermally driven reaction, with light only playing an auxiliary role. Indeed, the changes in light intensity and wavelength have no significant impact on product yield (Figures S10 and S11), further confirming the auxiliary effect of light. Moreover, the selectivity of the product did not reach 100%, mainly due to the peroxide reaction of toluene, generating by-products CO and CO_2 (Figure S12).[44] Fortunately, N-TiO_2-2 maintains nearly 90% photo-assisted thermal performance after 4 years of storage (Figure 5a), and the photo-assisted thermal performance of N-TiO_2-2 still remained 80% after five recycles, which represents an excellent stability. XRD, FT-IR, and TEM test results showed that the structure of N-TiO_2-2 remained unchanged after the reaction, and N doping was still uniformly distributed, further demonstrating its good stability (Figures S6, S13, and S14).

3.4. Catalytic Mechanism. N-TiO_2-2 has the highest concentrations of the O_V and Ti^{3+}, and it exhibited the optimal performance under thermal catalysis. Thereby, the optimal thermal performance may be due to the O_V and Ti^{3+}. O_V adsorbs and activates O_2 to produce superoxide radical ($\bullet O_2^-$), wherein the required electron (e^-) is from Ti^{3+}, and $\bullet O_2^-$ usually acts as active oxygen species for selective oxidation of toluene. Considering that the performance of N-TiO_2-2 was significantly enhanced under the condition of photo-assisted thermal catalysis, it may be that more e^- is generated by photoexcitation and then used by O_V to generate more $\bullet O_2^-$. Therefore, we have reason to believe that $\bullet O_2^-$ is active species for selective oxidation of toluene with N-TiO_2 and pristine TiO_2. Subsequently, the $\bullet O_2^-$ signal was detected for N-TiO_2 and pristine TiO_2 by EPR spectroscopy, wherein the strongest signal was detected for N-TiO_2-2, as expected (Figure 5b). The essential role of $\bullet O_2^-$ as active species was further verified by means of $\bullet O_2^-$ scavenger experiments. The thermal performance of N-TiO_2-2 was significantly inhibited by *p*-benzoquinone, and residual product yield and toluene conversion were only 4.8 mmol·g_{cat}^{-1} and 1786.7 μmol·g_{cat}^{-1}·h^{-1}, respectively (Figure 5c). In addition, the yield and toluene conversion of N-TiO_2-2 obtained under photo-assisted thermal catalysis were also decreased by 1.7 and 1.3 times after adding *p*-benzoquinone, respectively (Figure 5d). Furthermore, whether in thermal or photo-assisted thermal catalysis, the participation of e^- is essential in the formation of $\bullet O_2^-$, which was verified when potassium persulfate was added as an e^- quencher (Figure 5c,d). Moreover, the remaining hole (h^+) also appeared to play an essential role, since the product yield was significantly reduced when ammonium oxalate was added as a h^+ quencher (Figure 5c,d). Thus, $\bullet O_2^-$, e^-, and h^+ act together as active species to promote the selective oxidation of toluene.

The selective oxidation of toluene with N-TiO_2 and pristine TiO_2 is essentially thermally driven, whether under thermal or photo-assisted thermal catalysis, and the introduction of photoexcitation generates more active species without altering the original mechanism. Combined with the literature,[29,45,46] we suggest the catalytic mechanism as follows:

https://doi.org/10.1021/acsomega.3c01887
ACS Omega 2023, 8, 21026−21031

$$O_V + O_2 + e^- \rightarrow O_V + \bullet O_2^-$$

$$C_6H_5CH_3 + h^+ \rightarrow C_6H_5CH_2\bullet + H^+$$

$$C_6H_5CH_2\bullet + \bullet O_2^- \rightarrow C_6H_5CH_2OO^{\bullet -}$$

$$C_6H_5CH_2OO^{\bullet -} + H^+ \rightarrow C_6H_5CH_2OOH$$

$$C_6H_5CH_2OOH \rightarrow C_6H_5CHO + H_2O$$

$$2\,C_6H_5CH_2OOH \rightarrow 2\,C_6H_5CH_2OH + O_2$$

$$C_6H_5CH_2OH + 1/2 \bullet O_2^- \rightarrow C_6H_5CHO + H_2O$$

$$C_6H_5CHO + h^+ \rightarrow C_6H_5CO\bullet + H^+$$

$$C_6H_5CO\bullet + H^+ + 1/2 \bullet O_2^- \rightarrow C_6H_5COOH$$

$$C_6H_5COOH + C_6H_5CH_2OH \rightarrow C_6H_5CH_2OCOC_6H_5 + H_2O$$

4. CONCLUSIONS

Here, N-TiO_2 was prepared by a facile impregnation method, and more O_V and Ti^{3+} were achieved compared with pristine TiO_2. O_V and Ti^{3+} activate O_2 to generate $\bullet O_2^-$ as active species, and the resulting N-TiO_2-2 exhibited excellent thermal catalytic selective oxidation of toluene under solvent-free conditions. Its performance was further significantly enhanced, and more value-added products of toluene were obtained by photoexcitation, which attributed more active species generation benefitted from its best optical property. This highly efficient photo-assisted thermal catalysis demonstrates promising applications of noble-metal-free N-TiO_2 for those more challenging reactions.

■ ASSOCIATED CONTENT

Supporting Information

The Supporting Information is available free of charge at https://pubs.acs.org/doi/10.1021/acsomega.3c01887.

Characterization methods and instruments, SEM, TEM, Tauc plots, XPS valence band, time-resolved fluorescence decay, N atom concentration of the N-TiO_2, content of Ti^{3+} and O_v, specific activity value of N-TiO_2, and comparison of activity with other catalyst (PDF)

■ AUTHOR INFORMATION

Corresponding Author

Maoyong Song − *Key Laboratory of Environmental Nanotechnology and Health Effects and State Key Laboratory of Environmental Chemistry and Ecotoxicology, Research Center for Eco-Environmental Sciences, Chinese Academy of Sciences, Beijing 100085, China; University of Chinese Academy of Sciences, Beijing 100049, China;* orcid.org/0000-0002-6776-4705; Email: mysong@rcees.ac.cn

Authors

Cheng Chen − *Key Laboratory of Environmental Nanotechnology and Health Effects, Research Center for Eco-Environmental Sciences, Chinese Academy of Sciences, Beijing 100085, China; University of Chinese Academy of Sciences, Beijing 100049, China;* orcid.org/0000-0002-9439-0227

Mingge Wu − *Key Laboratory of Photochemistry, CAS Research/Education Center for Excellence in Molecular Sciences, Institute of Chemistry, Chinese Academy of Sciences, Beijing 100190, China*

Chunyan Ma − *Key Laboratory of Environmental Nanotechnology and Health Effects, Research Center for Eco-Environmental Sciences, Chinese Academy of Sciences, Beijing 100085, China*

Guibin Jiang − *University of Chinese Academy of Sciences, Beijing 100049, China; State Key Laboratory of Environmental Chemistry and Ecotoxicology, Research Center for Eco-Environmental Sciences, Chinese Academy of Sciences, Beijing 100085, China;* orcid.org/0000-0002-6335-3917

Complete contact information is available at: https://pubs.acs.org/10.1021/acsomega.3c01887

Notes

The authors declare no competing financial interest.

■ ACKNOWLEDGMENTS

This project was supported by the National Natural Science Foundation of China (grant no. 22125606) and the National Key R&D Program of China (2021YFA0910300).

■ REFERENCES

(1) Kesavan, L.; Tiruvalam, R.; Rahim, M. H. A.; Saiman, M. I. B.; Enache, D. I.; Jenkins, R. L.; Dimitratos, N.; Lopez-Sanchez, J. A.; Taylor, S. H.; Knight, D. W.; Kiely, C. J.; Hutchings, G. J. Solvent-free oxidation of primary carbon-hydrogen bonds in toluene using Au-Pd alloy nanoparticles. *Science* **2011**, *331*, 195−199.

(2) Li, X.; Wang, X.; Antonietti, M. Solvent-free and metal-free oxidation of toluene using O_2 and g-C_3N_4 with nanopores: nanostructure boosts the catalytic selectivity. *ACS Catal.* **2012**, *2*, 2082−2086.

(3) Punniyamurthy, T.; Velusamy, S.; Iqbal, J. Recent advances in transition metal catalyzed oxidation of organic substrates with molecular oxygen. *Chem. Rev.* **2005**, *105*, 2329−2364.

(4) Partenheimer, W. Methodology and scope of metal/bromide autoxidation of hydrocarbons. *Catal. Today* **1995**, *23*, 69−158.

(5) Suresh, A. K.; Sharma, M. M.; Sridhar, T. Engineering aspects of industrial liquid-phase air oxidation of hydrocarbons. *Ind. Eng. Chem. Res.* **2000**, *39*, 3958−3997.

(6) Singh, A. P.; Selvam, T. Liquid phase oxidation reactions over chromium silicalite-1 (CrS-1) molecular sieves. *J. Mol. Catal. A: Chem.* **1996**, *113*, 489−497.

(7) Zhou, W.; Huang, K.; Cao, M.; Sun, F.; He, M.; Chen, Z. Selective oxidation of toluene to benzaldehyde in liquid phase over CoAl oxides prepared from hydrotalcite-like precursors. *React. Kinet., Mech. Catal.* **2015**, *115*, 341−353.

(8) Song, G.; Feng, L.; Xu, J.; Zhu, H. Liquid-phase oxidation of toluene to benzaldehyde with molecular oxygen catalyzed by copper nanoparticles supported on graphene. *Res. Chem. Intermed.* **2018**, *44*, 4989−4998.

(9) Bastock, T. W.; Clark, J. H.; Martin, K.; Trenbirth, B. W. Mild, solvent-free oxidation of toluene and subsituted toluenes to their benzoic acids using carboxylic acidpromoted heterogeneous catalysis. *Green Chem.* **2002**, *4*, 615−617.

(10) Zhong, W.; Kirk, S. R.; Yin, D.; Li, Y.; Zou, R.; Mao, L.; Zou, G. Solvent-free selective oxidation of toluene by oxygen over MnO_x/SBA-15 catalysts: relationship between catalytic behavior and surface structure. *Chem. Eng. J.* **2015**, *280*, 737−747.

(11) Jiang, F.; Zhu, X.; Fu, B.; Huang, J.; Xiao, G. Au/γ-MnO_2 catalyst for solvent-free toluene oxidation with oxygen. *Chin. J. Catal.* **2013**, *34*, 1683−1689.

(12) Wang, F.; Xu, J.; Li, X.; Gao, J.; Zhou, L.; Ohnishi, R. Liquid phase oxidation of toluene to benzaldehyde with molecular oxygen

over copper−based heterogeneous catalysts. *Adv. Synth. Catal.* **2005**, *347*, 1987−1992.
(13) Li, X.; Xu, J.; Zhou, L.; Wang, F.; Gao, J.; Chen, C.; Ning, J.; Ma, H. Liquid-phase oxidation of toluene by molecular oxygen over copper manganese oxides. *Catal. Lett.* **2006**, *110*, 255−260.
(14) Li, X.; Lu, B.; Sun, J.; Wang, X.; Zhao, J.; Cai, Q. Selective solvent-free oxidation of toluene to benzaldehyde over zeolite supported iron. *Catal. Commun.* **2013**, *39*, 115−118.
(15) Fu, B.; Zhu, X.; Xiao, G. Solvent-free selective aerobic oxidation of toluene by ultra fine nano-palladium catalyst. *Appl. Catal., A* **2012**, *415*, 47−52.
(16) Liu, Y.; Chen, L.; Yuan, Q.; He, J.; Au, C.; Yin, S. A green and efficient photocatalytic route for the highly-selective oxidation of saturated alpha-carbon C−H bonds in aromatic alkanes over flower-like Bi_2WO_6. *Chem. Commun.* **2016**, *52*, 1274−1277.
(17) Langhammer, D.; Kullgren, J.; Österlund, L. Photoinduced adsorption and oxidation of SO_2 on anatase TiO_2 (101). *J. Am. Chem. Soc.* **2020**, *142*, 21767−21774.
(18) Liu, G.; Yin, L.; Wang, J.; Niu, P.; Zhen, C.; Xie, Y.; Cheng, H. A red anatase TiO_2 photocatalyst for solar energy conversion. *Energy Environ. Sci.* **2012**, *5*, 9603−9610.
(19) Zhu, M.; Lai, J.; Tumuluri, U.; Wu, Z.; Wachs, I. E. Nature of active sites and surface intermediates during SCR of NO with NH_3 by supported V_2O_5−WO_3/TiO_2 catalysts. *J. Am. Chem. Soc.* **2017**, *139*, 15624−15627.
(20) Zhang, Y.; Liu, J.; Qian, K.; Jia, A.; Li, D.; Shi, L.; Hu, J.; Zhu, J.; Huang, W. Structure Sensitivity of Au-TiO_2 Strong Metal−Support Interactions. *Angew. Chem., Int. Ed.* **2021**, *60*, 12074−12081.
(21) Shekhar, M.; Wang, J.; Lee, W. S.; Williams, W. D.; Kim, S. M.; Stach, E. A.; Miller, J. T.; Delgass, W. N.; Ribeiro, F. H. Size and support effects for the water−gas shift catalysis over gold nanoparticles supported on model Al_2O_3 and TiO_2. *J. Am. Chem. Soc.* **2012**, *134*, 4700−4708.
(22) Xie, J.; Jin, R.; Li, A.; Bi, Y.; Ruan, Q.; Deng, Y.; Zhang, Y.; Yao, S.; Sankar, G.; Ma, D.; Tang, J. Highly selective oxidation of methane to methanol at ambient conditions by titanium dioxide-supported iron species. *Nat. Catal.* **2018**, *1*, 889−896.
(23) Zhang, X.; Shi, R.; Li, Z.; Zhao, J.; Huang, H.; Zhou, C.; Zhang, T. Photothermal-assisted photocatalytic nitrogen oxidation to nitric acid on palladium-decorated titanium oxide. *Adv. Energy Mater.* **2022**, *12*, 2103740−2103746.
(24) Pan, X.; Yang, M.; Fu, X.; Zhang, N.; Xu, Y. Defective TiO_2 with oxygen vacancies: synthesis, properties and photocatalytic applications. *Nanoscale* **2013**, *5*, 3601−3614.
(25) Liu, N.; Xu, M.; Yang, Y.; Zhang, S.; Zhang, J.; Wang, W.; Zheng, L.; Hong, S.; Wei, M. $Au^{\delta-}$−O_v−Ti^{3+} interfacial site: catalytic active center toward low-temperature water gas shift reaction. *ACS Catal.* **2019**, *9*, 2707−2717.
(26) Li, P.; Zhang, Z.; Zhuang, Z.; Guo, J.; Fang, Z.; Fereja, S. L.; Chen, W. Pd-doping-induced oxygen vacancies in one-dimensional tungsten oxide nanowires for enhanced acetone gas sensing. *Anal. Chem.* **2021**, *93*, 7465−7472.
(27) Wang, Z.; Du, Y.; Dohnálek, Z.; Lyubinetsky, I. Direct observation of site-specific molecular chemisorption of O_2 on TiO_2 (110). *J. Phys. Chem. Lett.* **2010**, *1*, 3524−3529.
(28) Chen, C.; Wu, M.; Yang, C.; Yu, X.; Yu, J.; Yin, H.; Li, G.; Su, G.; Hao, Z.; Song, M.; Ma, C. Electron-donating N^{-}−Ti^{3+}−O_v interfacial sites with high selectivity for the oxidation of primary C−H bonds. *Cell Rep. Phys. Sci.* **2022**, *3*, No. 100936.
(29) Cao, X.; Chen, Z.; Lin, R.; Cheong, W. C.; Liu, S.; Zhang, J.; Peng, Q.; Chen, C.; Han, T.; Tong, X.; Wang, Y.; Shen, R.; Zhu, W.; Wang, D.; Li, Y. A photochromic composite with enhanced carrier separation for the photocatalytic activation of benzylic C−H bonds in toluene. *Nat. Catal.* **2018**, *1*, 704−710.
(30) Du, S.; Bian, X.; Zhao, Y.; Shi, R.; Zhang, T. Progress and prospect of photothermal catalysis. *Chem. Res. Chin. Univ.* **2022**, *38*, 723−734.
(31) Appadurai, T.; Subramaniyam, C. M.; Kuppusamy, R.; Karazhanov, S.; Subramanian, B. Electrochemical performance of nitrogen-doped TiO_2 nanotubes as electrode material for supercapacitor and Li-ion battery. *Molecules* **2019**, *24*, 2952.
(32) Singh, P.; Sinha, O. P.; Srivastava, R.; Srivastava, A. K.; Bindra, J. K.; Singh, R. P.; Kamalasanan, M. N. Studies on morphological and optoelectronic properties of MEH-CN-PPV: TiO_2 nanocomposites. *Mater. Chem. Phys.* **2012**, *133*, 317−323.
(33) Dai, S.; Wu, Y.; Sakai, T.; Du, Z.; Sakai, H.; Abe, M. Preparation of highly crystalline TiO_2 nanostructures by acid-assisted hydrothermal treatment of hexagonal-structured nanocrystalline titania/cetyltrimethyammonium bromide nanoskeleton. *Nanoscale Res. Lett.* **2010**, *5*, 1829−1835.
(34) Du, J.; Zhao, G.; Shi, Y.; Yang, H.; Li, Y.; Zhu, G.; Mao, Y.; Sa, R. J.; Wang, W. A facile method for synthesis of N-doped TiO_2 nanooctahedra, nanoparticles, and nanospheres and enhanced photocatalytic activity. *Appl. Surf. Sci.* **2013**, *273*, 278−286.
(35) Li, Y.; Peng, Y.; Hu, L.; Zheng, J.; Prabhakaran, D.; Wu, S.; Puchtler, T. J.; Li, M.; Wong, K. Y.; Taylor, R. A.; Tsang, S. C. E. Photocatalytic water splitting by N-TiO_2 on MgO (111) with exceptional quantum efficiencies at elevated temperatures. *Nat. Commun.* **2019**, *10*, 1−9.
(36) Valentin, C. D.; Pacchioni, G.; Selloni, A.; Livraghi, S.; Giamello, E. Characterization of paramagnetic species in N-doped TiO_2 powders by EPR spectroscopy and DFT calculations. *J. Phys. Chem. B* **2005**, *109*, 11414−11419.
(37) Jiang, J.; Xing, Z.; Li, M.; Li, Z.; Wu, X.; Hu, M.; Wan, J.; Wang, N.; Besov, A. S.; Zhou, W. In situ Ti^{3+}/N-codoped three-dimensional (3D) urchinlike black TiO_2 architectures as efficient visible-light-driven photocatalysts. *Ind. Eng. Chem. Res.* **2017**, *56*, 7948−7956.
(38) Zhao, Z.; Goncalves, R. V.; Barman, S. K.; Willard, E. J.; Byle, E.; Perry, R.; Wu, Z.; Huda, M. N.; MouléA, J.; Osterloh, F. E. Electronic structure basis for enhanced overall water splitting photocatalysis with aluminum doped $SrTiO_3$ in natural sunlight. *Energy Environ. Sci.* **2019**, *12*, 1385−1395.
(39) Xu, Y.; Wu, S.; Wan, P.; Sun, J.; Hood, Z. D. Introducing Ti^{3+} defects based on lattice distortion for enhanced visible light photoreactivity in TiO_2 microspheres. *RSC Adv.* **2017**, *7*, 32461−32467.
(40) Zhang, B.; Wang, L.; Zhang, Y.; Ding, Y.; Bi, Y. Ultrathin FeOOH nanolayers with abundant oxygen vacancies on $BiVO_4$ photoanodes for efficient water oxidation. *Angew. Chem., Int. Ed.* **2018**, *57*, 2248−2252.
(41) Lian, Z.; Wang, W.; Li, G.; Tian, F.; Schanze, K. S.; Li, H. Pt-enhanced mesoporous Ti^{3+}/TiO_2 with rapid bulk to surface electron transfer for photocatalytic hydrogen evolution. *ACS Appl. Mater. Interfaces* **2017**, *9*, 16959−16966.
(42) Wan, J.; Chen, W.; Jia, C.; Zheng, L.; Dong, J.; Zheng, X.; Wang, Y.; Yan, W.; Chen, C.; Peng, Q.; Wang, D.; Li, Y. Defect effects on TiO_2 nanosheets: stabilizing single atomic site Au and promoting catalytic properties. *Adv. Mater.* **2018**, *30*, 1705369.
(43) Pei, D.; Gong, L.; Zhang, A.; Zhang, X.; Chen, J.; Mu, Y.; Yu, H. Defective titanium dioxide single crystals exposed by high-energy {001} facets for efficient oxygen reduction. *Nat. Commun.* **2015**, *6*, 1−10.
(44) Shu, Y.; Liang, S.; Xiao, J.; Tu, Z.; Huang, H. Phosphate-and Mn-modified mesoporous TiO_2 for efficient catalytic oxidation of toluene in VUV-PCO system. *Acta Phys.-Chim. Sin.* **2021**, *37*, 2010001.
(45) Yuan, R.; Fan, S.; Zhou, H.; Ding, Z.; Lin, S.; Li, Z.; Zhang, Z.; Xu, C.; Wu, L.; Wang, X.; Fu, X. Chlorine-Radical-Mediated Photocatalytic Activation of C-H Bonds with Visible Light. *Am. Ethnol.* **2013**, *125*, 1069−1073.
(46) Guo, C.; Liu, Q.; Wang, X.; Hu, H. Selective liquid phase oxidation of toluene with air. *Appl. Catal., A* **2005**, *282*, 55−59.

https://doi.org/10.1021/acsomega.3c01887
ACS Omega 2023, 8, 21026−21031